Check for updates

Hindawi Publishing Corporation
International Journal of Distributed Sensor Networks
Volume 2012, Article ID 406710, 12 pages
doi:10.1155/2012/406710

Research Article

A Robust Baseband Demodulator for ISO 18000-6C RFID Reader Systems

Cheng Jin and Sung Ho Cho

Department of Electronics and Computer Engineering, Hanyang University, Seoul 133-791, Republic of Korea

Correspondence should be addressed to Cheng Jin, skim0002012@gmail.com

Received 25 April 2012; Accepted 23 July 2012

Academic Editor: Minglu Li

Copyright © 2012 C. Jin and S. H. Cho. This is an open access article distributed under the Creative Commons Attribution License, which permits unrestricted use, distribution, and reproduction in any medium, provided the original work is properly cited.

One key challenge for ultra-high frequency (UHF) radio-frequency identification (RFID) reader design is to demodulate the weak tag response signal which tends to be easily distorted and has considerable frequency deviations. In this paper, a baseband demodulator based on a matched filter (MF) is proposed to enhance the reliability of signal processing for the EPCglobal Class-1 Generation-2 (Gen2) RFID reader systems. The proposed demodulator is very robust against strong signal distortions and large frequency deviations happening on the received backscattered signal from a passive RFID tag. The validity and usefulness is demonstrated by both computer simulations and implementation experiments.

1. Introduction

Radio-frequency identification (RFID) is an automatic wireless identification technology which has become an attractive solution for supply chain management and industry automation. In particular, the use of passive UHF RFID tag has received a tremendous amount of attention for its capability to function without a battery and its low manufacture cost. The ISO/IEC 18000-6C protocol, which is also known as the EPCglobal Class-1 Generation-2 protocol (hereafter referred to as the Gen2 protocol), is an air interface specification adopted by the industry for UHF (860–960 MHz) RFID systems. This protocol defines the physical and logical specifications for a passive-backscatter, reader-talks-first (RTF), RFID system operating in the 860–960 MHz frequency range.

The passive-backscatter, RTF based system faces a variety of problems, including frequency deviation and signal distortion of the tag-backscattered signal. At the receiver of an RFID reader, the tag-backscattered signal has a very weak power and can be easily distorted when passing through a power amplifier, a bandpass filter, or an analog-to-digital converter (ADC). The signal-to-noise ratio (SNR) is thus very low sometimes especially in dense-reader environment where interferences by other nearby working readers, present. Hence, demodulation of the weak tag-backscattered signal in the presence of distortion and frequency deviation is a key challenge in the design of an RFID reader.

2. Related Works

Conventional digital receivers based on a zero-crossing demodulator (ZCD) were proposed in [1, 2] and have been widely employed in wireless communication systems for their efficiency and simplicity [3–7]. The ZCD has also been commonly used in the receivers of RFID readers [8–13]. Although the ZCD provides efficiency and simplicity, there is a problem that its performance highly depends on the accurate zero crossing information. For noise reduction, a lowpass filter or bandpass filter is usually utilized before the ZCD [8]. These highly computational filtering methods remove white noise, however, cannot effectively eliminate signal distortion. In addition, they are very sensitive to frequency deviations and have limited operating frequency ranges. In passive RFID systems, there are considerable frequency deviations present, and the received signal can be easily distorted. Therefore, the expected performance or reliability of the ZCD can often be degraded.

Besides the ZCD, demodulator structures basing on correlations instead of the ZCD for an RFID reader have been presented in [14, 15]. In these works, the maximum-likelihood (ML) detector for frequency deviation estimation has been proposed. However, practical channel disturbances, like the amplitude distortions, were not taken into consideration. The expected reliability of these works cannot be guaranteed in practical environments.

In this paper, we focus on dealing with the signal distortion and frequency deviation happening on a tag-backscattered signal in UHF RFID systems, and propose a matched filter (MF) based baseband demodulator for the RFID reader to enhance the reliability in practical environments. The proposed baseband demodulator is made up of: (i) an MF to compensate for signal distortion and (ii) a symbol detector based on ML estimation of frequency deviation.

The remainder of this paper is organized as follows. Section III discusses the challenges specific to the reader receiver design in passive UHF RFID systems. Section IV describes the system model. Section V presents the proposed baseband MF demodulator. Section VI provides performance evaluation results by computer simulation. Section VII describes the detailed implementation issues and provides experiment results. In Section VIII, the conclusions are drawn.

3. Signal Processing Challenges in Passive UHF RFID Systems

3.1. RFID System Overview. An RFID system generally consists of an RFID reader and one or more RFID tags. In UHF RFID systems, since tags are passive and contain no independent power source such as a battery, the operating power is harvested from the incoming RF field transmitted by the reader. In the operation of the system, the reader initiates an inventory round (the time required to identify all tags within a field) by transmitting an unmodulated continuous-wave (CW) RF signal in the 860 MHz–960 MHz frequency range to power up the tags. Once the tags are energized, the reader transmits a command to the tags by modulating the RF signal. After the reader completes the command transmission, it continues to send a CW RF signal to the tags. On receiving the command and operating power from the reader, the tag responds by changing the reflection coefficient of its antenna, thereby backscattering an information signal to the reader. The tag backscattering signal is so weak that the power difference between the reader's transmitted signal and received tag backscattering signal could be up to 90 dB at the reader for a reader-to-tag distance of 2 m. Therefore, if there is another operating reader present nearby, the interfering signal could overwhelm the small tag-backscattering signal, thus prevent us from successfully demodulating the tag signal.

3.2. Signal Distortion. In an environment of dense reader mode (DRM) [16], most or all of the available channels are occupied by simultaneously active readers (e.g., 25 readers operating in 25 available channels). To prevent reader transmissions from colliding with tag responses, numerous frequency-division multiplexing (FDM) methods are suggested in [16]. In these methods, reader transmissions and tag responses are separated into different channels to minimize reader-on-tag interferences. Figure 1 illustrates an example of channelization for DRM by European Telecommunications Standards Institute (ETSI) [17]. In the ETSI regulation, 10 channels of 200 kHz each in the range of 865 MHz to 868 MHz are allocated, and readers are allowed to transmit in channels 4, 7, 10, and 13. Channel separation is enforced since the power of a tag response is so weak that a reader transmission in an adjacent channel can overwhelm tag responses.

Despite the fact that interferences from other readers do not occupy the same channel used by tag responses simultaneously, the large difference in signal strength would result in poor reception of tag responses at a reader. Thus, a bandpass filter (as shown in Figure 1) which filters interfering readers from desired tag responses is required to implement at the reader. Since creating a bandpass filter in digital domain imposes a high requirement for dynamic range and resolution of an ADC, the bandpass filter is generally implemented as a baseband analog filter. Despite the advantages of analog filters such as high speed and large dynamic range, the performance of analog filters is limited by the accuracy of imperfect electronic components. Figure 2 shows the frequency response comparison between a digital FIR filter and three most commonly used analog filters in RFID systems: Butterworth, Chebyshev, and Elliptic [10, 18]. The frequency response is for a bandpass filter which provides a bandwidth limitation of 300 kHz specified in the DRM regulations. As shown in Figure 2, comparing with the nearly ideal response of a digital filter, the analog filters have more passband ripples, slower transition rolloff, and lower stop-band attenuation.

Under the strict bandwidth limitation required for creating a clean signal in DRM environment, these nonideal performance characteristics of analog filters could cause distortion of the tag response signal. Figure 3 shows the filtering results of a tag-response signal backscattered on a link frequency of 300 kHz, Miller-4 subcarrier using the analog filters. In Figure 3, the original tag-response signal is a Miller-4-modulated subcarrier sequence, which contains 4 subcarrier cycles per bit ($M = 4$). According to Miller modulation characteristics, there are subcarrier cycles without phase inversion in the middle of the cycle [16]. In spite of a small percent of the total, these subcarriers represent a frequency component at 150 kHz, which is half of the backscatter link frequency.

Residing on the boundary of the bandwidth limitation, these subcarriers tend to be easily distorted by the nonideal analog bandpass filters. The subcarriers distorted by the 4^{th}-order analog filters are shown in Figure 3. As can be seen, despite the characteristic differences between different analog filters, there are always some signal distortions induced by the filtering.

Apart from the DRM environment, the weak tag-backscattering signal can be easily distorted when passing through a nonlinear amplifier, or an analog-to-digital

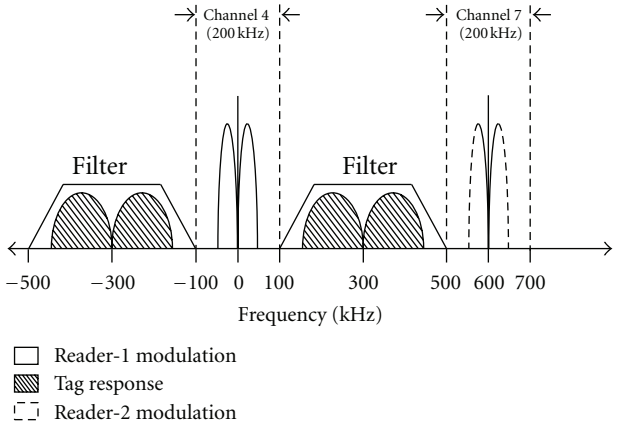

Figure 1: Channelization for DRM environment.

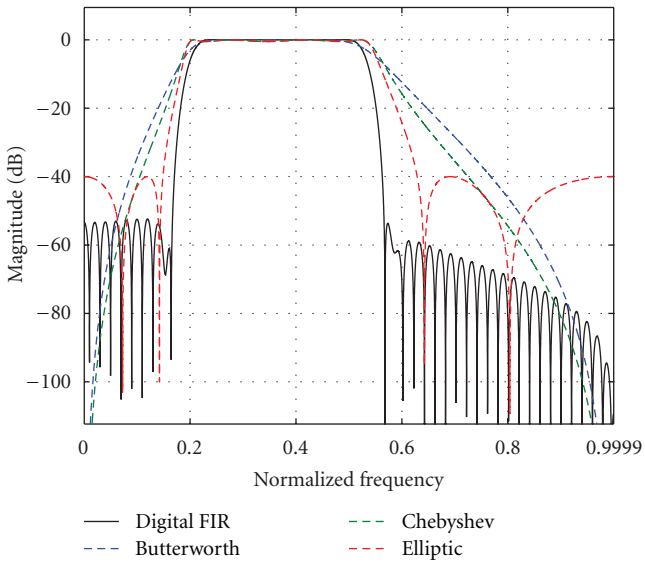

Figure 2: Frequency response of a bandpass filter for DRM environment.

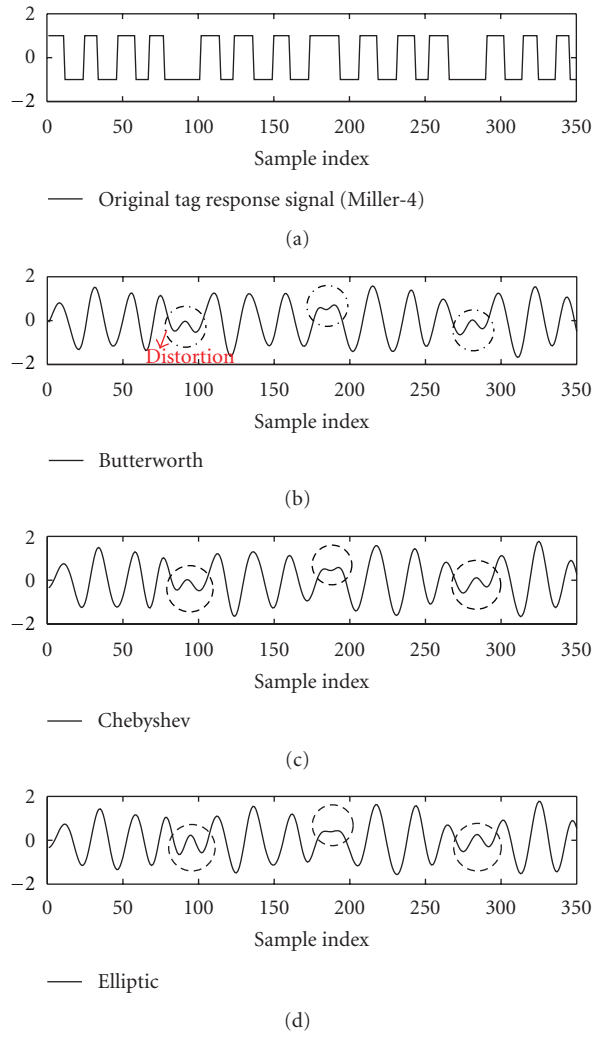

Figure 3: Signal distortion caused by analog filters (tag response signal at backscatter link frequency of 300 kHz, Miller-4 subcarrier).

converter (ADC) at the reader receiver. In this paper, it is assumed that the signal distortion caused by nonlinear amplifier and ADC can be removed by some methods. We focus on the signal distortion caused by the nonideal bandpass filter which can contribute more undesirable effects to the signal distortion problem. The signal distortion can lead to performance degradation of the conventional baseband demodulators.

3.3. Frequency Deviation. According to the Gen2 standard, a tag is specified to respond with a backscatter-link frequency (BLF) ranging from 40 kHz to 640 kHz. In addition, a frequency deviation of up to ±22% of the nominal BLF is permitted. Frequency deviation describes difference between an actual frequency and nominal frequency, as shown in Figure 4. Frequency deviation is mainly caused by the phase noise of oscillators, which can lead to dramatic changes in oscillator's frequency spectrum.

In UHF RFID systems, since passive tags have no internal power supply, the internal clock used in the tag is extracted from the incoming RF signal. For generating the internal clock, a relaxation or a ring oscillator is generally used [19]. These oscillators are efficient in backscattering performance; however, have heavy phase noise. The unavoidable phase noise leads to the large frequency deviations in the tag backscattering signal. Since the exact frequency deviation is unknown to the reader, the unpredictable large frequency deviation brings difficulty to frequency estimation and symbol synchronization of the tag signal.

These specific characteristics of the tag-backscattered signal, such as signal distortion and frequency deviation, make demodulation of the tag-response signal a difficult task.

4. System Model

The basic uplink (tag-to-reader) communication structure of a passive RFID system can be described as follows. When

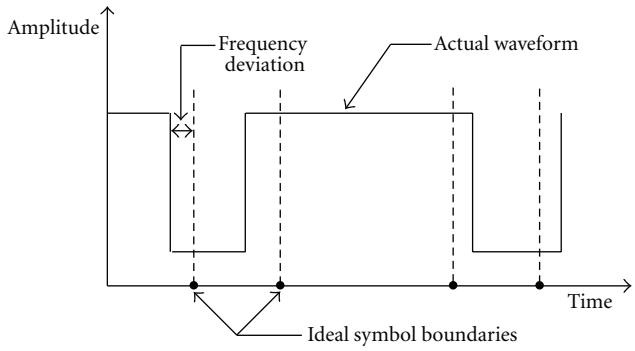

Figure 4: Frequency deviation in the tag-backscattering response signal.

a tag gets ready to send a reply signal to the reader, the information binary bits are encoded into baseband symbols $\{a_n\} \in \{+1, -1\}$ $(n = 0, 1, 2, \ldots, N-1)$ by certain line coding scheme like FM0 or Miller [16]. In this paper, the Miller code is used as a default. Thus the baseband modulated signal sent by the tag can be represented as

$$s(t) = \sum_{n=0}^{N-1} a_n h(t - nT), \tag{1}$$

where $\{a_n\}$ are the Miller coded baseband symbols, T is the symbol period and $h(\cdot)$ is the symbol pulse shape defined as

$$h(t) = \begin{cases} A, & |t| < \dfrac{T}{2}, \\ 0, & |t| \geq \dfrac{T}{2}. \end{cases} \tag{2}$$

Since a relaxation or a ring oscillator is generally used for generating clock in passive RFID tags, phase noise exists in the actual generated baseband signal $s'(t)$, which can be expressed as

$$s'(t) = \sum_{n=0}^{N-1} a_n h(t - nT + \sigma(t)T), \tag{3}$$

where $\sigma(t)$ is the phase noise whose effect is to create a deviation in the transition time of the square waves [20].

As shown in Figure 5, at the receiver side of the reader, the tag-backscattering signal passes through an LNA, a mixer, and a bandpass filter (BPF). We use $x(t)$ to describe the received tag-backscattering signal before passing the BPF and $x(t)$ can be expressed as

$$x(t) = s'(t) + n_0(t), \tag{4}$$

where $n_0(t)$ indicates the received noise of additive white Gaussian noise (AWGN). Since we focus on the signal distortion caused by the nonideal analog filter, thus, we assume the BPF in Figure 5 makes signal distortion to $x(t)$. We use $y(t)$ to indicate the distorted version of $x(t)$ by passing through the BPF, and $y(t)$ is expressed as

$$\begin{aligned} y(t) &= x(t) * d(t) \\ &= (s'(t) + n_0(t)) * d(t) \\ &= d(t) * \sum_{n=0}^{N-1} a_n h(t - nT + \sigma(t)T) + n(t), \end{aligned} \tag{5}$$

where $d(t)$ indicates the distortion signal caused by the BPF, $n(t)$ indicates the distorted version of $n_0(t)$ by $d(t)$. $y(t)$ in (5) is the final received distorted signal, which is also the input signal to the Baseband demodulator for demodulation. The distortion signal $d(t)$ is modeled as a digital FIR filter, the ideal impulse response of which is

$$D_{\mathrm{BF}}(j\omega) = \begin{cases} 1, & 2\pi(f_0 - f_L) \leq |\omega| \leq 2\pi(f_0 + f_H), \\ 0, & \text{otherwise}, \end{cases} \tag{6}$$

where f_0 is the center frequency, f_L is the lower pass-band frequency, and f_H is the upper pass-band frequency.

Since the typical wide and deep amplitude distortion is our main concern, for quantifying the distortion level, we define a parameter of distortion-to-signal ratio—DS—as

$$\mathrm{DS} = \frac{E_{\mathrm{sd}}}{E_s} = \frac{\int_0^T (s'(t) * d(t))^2}{\int_0^T s'^2(t)}, \tag{7}$$

where E_{sd} represents the power of the distorted signal $s'(t) * d(t)$, E_s represents the power of the original undistorted signal $s'(t)$. The target signal is the baseband Miller-4 modulated signal with BLF as well as bandwidth (BW) at 300 kHz, and maximum frequency deviation at ±%22.

For obtaining the effect of amplitude distortion, we choose the method of decreasing the passband of the filter $D_{\mathrm{BF}}(j\omega)$. For example, at f_H = BW/2, we change f_L from BW/2 to $BW/4$, and BW/8. In this way, an increasing level of amplitude distortion can be obtained. Figure 6 shows the distorted signal with different levels of distortion measured by DS defined in (7).

5. Proposed Baseband MF Demodulator

The architecture of the proposed Baseband MF demodulator is shown in Figure 5, which consists of two parts: the matched filter and the symbol detector.

5.1. Matched Filter. It is known that the MF is the optimal linear filter to provide the maximum signal-to-noise ratio (SNR) at its output for a known transmitted symbol waveform in the presence of additive stochastic noise. For achieving desired performance, the MF should be matched to the received pulse rather than the transmitted pulse. In practice, the transmitted signal is not always composed of a single pulse shape, like the Miller-coded signal. Furthermore, in practice, intersymbol interference (ISI) and nonlinearities would contribute to produce a distorted version of the transmitted pulse at the receiver. The MF can contribute

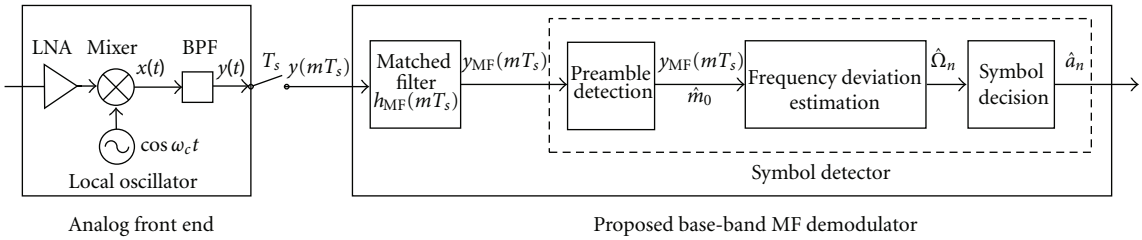

Figure 5: Architecture of the proposed Baseband MF demodulator.

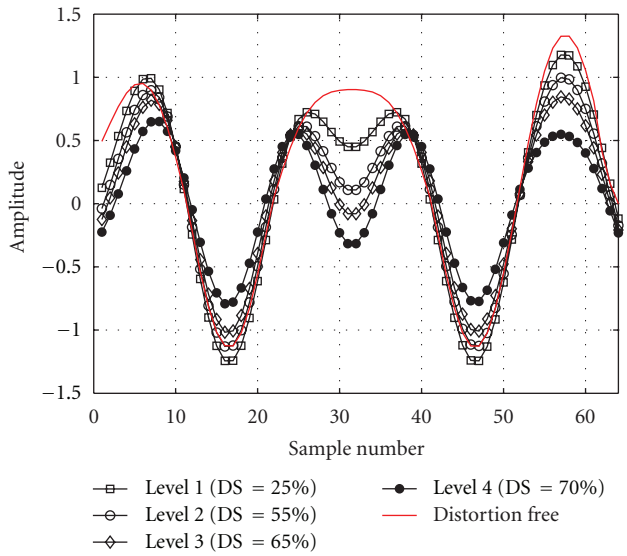

Figure 6: Different levels of amplitude distortion.

to compensating for some signal distortions in pulses when the distortion is known. In this paper, we use the MF to compensate for the amplitude distortion caused by the nonideal analog filters.

As shown in Figure 5, by sampling the received tag signal $y(t)$ at a sampling interval of T_S, we get $y(mT_S)$. Note that due to the interference of phase noise $\sigma(t)$, a time period of $\sigma(t)T$, which causes the frequency deviation, is induced into the pulse of $h(t)$, as expressed in (3). We use $\Delta\varepsilon_n T_S$ to represent the sampling result of $\sigma(t)T$. Then, we get [21] the following:

$$y(mT_S) = \sum_{m=0}^{\infty}\left[d(mT_S) * \sum_{n=0}^{N-1} a_n h((m - nM + \Delta\varepsilon_n)T_S) + n(mT_S)\right], \tag{8}$$

where m is the sample index, M is the number of samples in the pulse duration of T, and $\Delta\varepsilon_n$ is the number of samples by sampling $\sigma(t)$ in the nth pulse.

The ideal MF is expected to match each pulse shape $h(\cdot)$ in (8) including the frequency deviation of $\Delta\varepsilon_n T_S$. However, at this stage, the exact information of $\Delta\varepsilon_n T_S$ is not available. We use $\Delta\bar{\varepsilon}$, an average of $\Delta\varepsilon_n$ calculated from a number of pulses using the moving average method, instead of $\Delta\varepsilon_n$ in the proposed MF. Thus, the proposed MF is expressed as

$$h_{\mathrm{MF}}(mT_S) = \begin{cases} A, & 0 \le m \le M + \Delta\bar{\varepsilon}, \\ 0, & \text{otherwise.} \end{cases} \tag{9}$$

The proposed MF in (9) is not exactly matched to the pulse $h(\cdot)$ in (8); however, since our main concern is to compensate for the amplitude distortion, the further frequency deviation caused by the MF is proposed to be detected by the frequency deviation estimator in the symbol detector (shown in Figure 5). The output of the MF, $y_{\mathrm{MF}}(mT_S)$ is

$$y_{\mathrm{MF}}(mT_S) = \sum_{m=0}^{\infty}\left[\sum_{k=0}^{M+\Delta\bar{\varepsilon}} h_{\mathrm{MF}}(kT_S) \cdot y(mT_S - kT_S)\right]. \tag{10}$$

Figure 7 shows the effect of the proposed MF on the amplitude distorted signal.

The distorted signal is generated with BLF at 300 kHz, maximum frequency deviation at ±22%, and distortion level DS at 70%. The average frequency deviation $\Delta\bar{\varepsilon}$ applied is $22\% \times (T/T_S)$. We observe effect in both frequency domain and time domain. As shown in Figure 7(a), the SNR of the filtered signal is obviously increased. Figure 7(b) shows the result in time domain, and it can be seen that the serious amplitude distortions exceeding beyond the zero-crossing threshold are effectively compensated.

5.2. Symbol Detector. After compensating for the amplitude distortions, the signal will be decoded by the symbol detector. As shown in Figure 5, the symbol detector consists of three parts: preamble detection, frequency deviation estimation, and symbol decision. The start position $\hat{m}_0$ of the useful data to be decoded can be detected by searching the known preamble pattern in $y_{\mathrm{MF}}(mT_S)$. For symbol detection, we propose a maximum-likelihood (ML) approach to estimate the frequency deviation of each symbol and achieve symbol synchronization.

In Miller-coding scheme, a "0" is coded with a transition in the half symbol duration, and a "1" is coded with a lack of transition. Decided by the start state of each symbol, the pattern is inverted. We use $s^k(t)$ $(k = 1, 2, 3, 4)$ to express the waveform for a Miller symbol, which for a data "0" is given by

$$s^1(t) = \begin{cases} 1, & 0 \le t \le T, \\ -1, & T < t \le 2T, \end{cases} \qquad s^2(t) = -s^1(t), \tag{11}$$

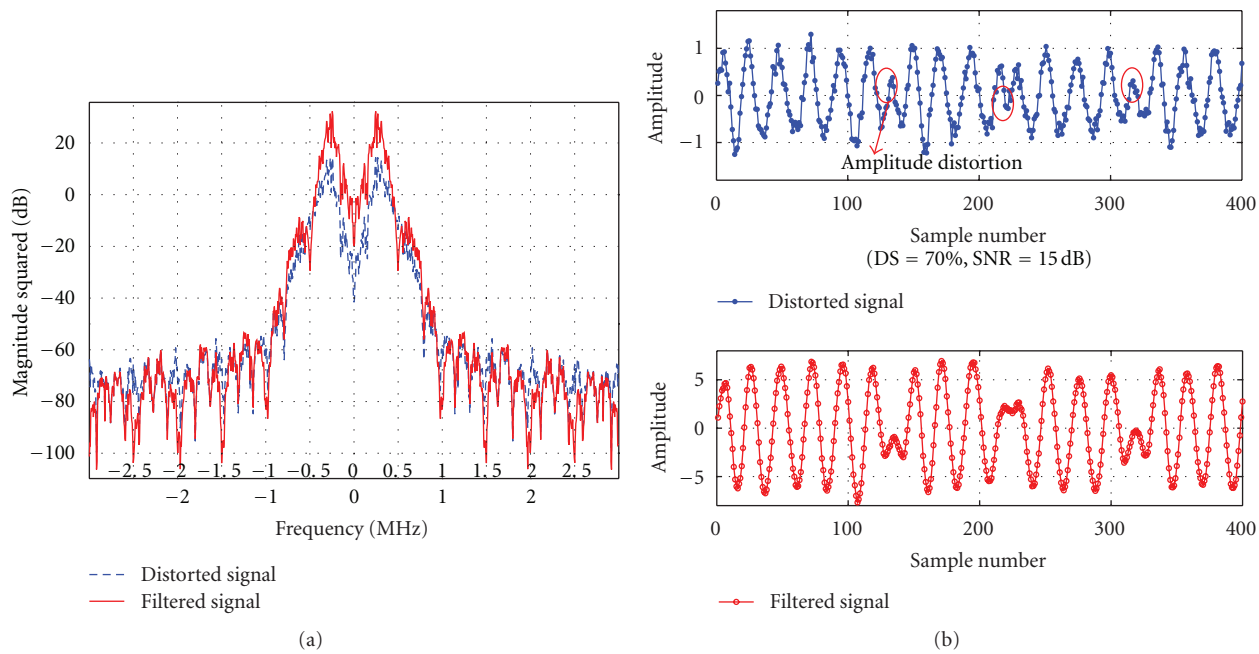

Figure 7: MF's effect on amplitude distortions: (a) frequency domain observation; (b) time domain observation.

and for a data "1" is given by

$$s^3(t) = 1, \quad 0 \le t \le 2T, \quad s^4(t) = -s^3(t), \tag{12}$$

where T is the pulse duration of the original symbol defined in (1). In the presence of frequency deviation $\sigma(t)T$ described in the last section, we model the symbol waveform (data "0" for example) of $s^1(t)$ with frequency deviation in a digital form as

$$s^1_\Omega(mT_S) = \begin{cases} 1, & 0 \le m \le M + \Delta\varepsilon_1, \\ -1, & M + \Delta\varepsilon_1 < m \le 2M + \Delta\varepsilon_1 + \Delta\varepsilon_2. \end{cases} \tag{13}$$

where M is the number of samples in the original pulse duration of T, $\Delta\varepsilon_1$ and $\Delta\varepsilon_2$, are the number of samples of the frequency deviation $\sigma_1(t)$ and $\sigma_2(t)$ in the first and second half of the symbol period, respectively. The range of $\Delta\varepsilon_1$ and $\Delta\varepsilon_2$ is determined by the maximum frequency deviation, which is defined as the frequency tolerance (FT) [16], and $\Delta\varepsilon_{\max} = |\text{round}(M \times \text{FT})|$, and

$$|\Delta\varepsilon_1| \le \Delta\varepsilon_{\max}, \qquad |\Delta\varepsilon_2| \le \Delta\varepsilon_{\max}. \tag{14}$$

For example, when $M = 10$ (10 samples in a pulse duration of T) and FT $= \pm\%22$, then $\Delta\varepsilon_{\max} = |\text{round}(10 \times 22\%)| = 2$. If the exact values of $\Delta\varepsilon_1$ and $\Delta\varepsilon_2$ are detected, then the actual symbol length of $s^1_\Omega(\cdot)$—Ω, can be determined as

$$\Omega = 2M + \Delta\varepsilon_1 + \Delta\varepsilon_2. \tag{15}$$

For detecting the exact values of $\Delta\varepsilon_1$ and $\Delta\varepsilon_2$, an ML function is performed at the frequency deviation estimation block (shown in Figure 5), which can be expressed as

$$\hat{\Omega}_n = \arg\max_m \sum_{m=0}^{2M+\Delta\varepsilon_1+\Delta\varepsilon_2} y_{\text{MF}}\left[\left(\hat{m}_0 + m + \hat{\Omega}_{n-1}\right)T_S\right] \cdot s^k_\Omega(mT_S), \tag{16}$$

Table 1: Basic system parameters used in the simulation.

Channel	Down-link rate	Up-link frequency	|FT|	Encoding method	EPC length
AWGN, amplitude distortion	40 kbps	300 kHz	22%	Miller-4	96 bits

where $\hat{\Omega}_n$ and $\hat{\Omega}_{n-1}$ are the estimated symbol lengths for the nth, $(n-1)$th symbol, respectively, and k is the possible type of symbol waveform $k \in \{1, 2, 3, 4\}$. Basing on the estimated symbol length $\hat{\Omega}_n$ and the symbol type k, a recovered Baseband symbol $\hat{a}_n$ can be obtained at the output of the symbol decision block shown in Figure 5.

6. Performance Evaluation Results by Simulation

In this section, we evaluate the performance of the proposed baseband MF demodulator and compare it with the conventional zero-crossing demodulator (ZCD) [8] and the correlation (CORR) demodulator [14]. A baseband Gen2 RFID system in an AWGN channel embedded with amplitude distortions is modeled by simulation. The basic parameters of the system are listed in Table 1. The anticollision algorithm and timing specifications used in the simulation can be found in [16].

According to the Gen2 protocol, the tag identification procedure can be simply described as follows. Firstly, the reader issues a *Query* command which contains a Q parameter to define a number as $2^Q - 1$. Then each tag receiving the *Query* command randomly selects a slot number (SN)

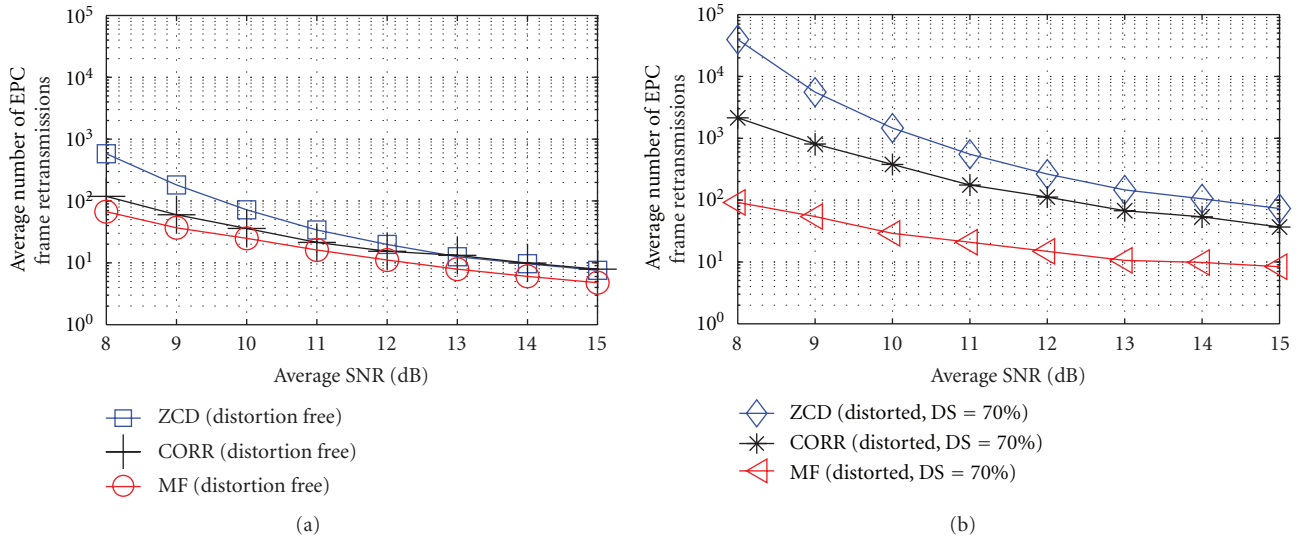

Figure 8: Average number of EPC frame retransmissions: (a) no signal distortion; (b) signal distorted.

in the range of $[0, 2^Q - 1]$. Only the tag whose SN is zero responds to the reader by sending an *RN16*, a 16-bit random number. If the reader correctly decodes the *RN16*, it sends back an *ACK* command which contains the same *RN16* to the tag. If the tag's *RN16* is the same with that in the *ACK* command, it sends its ID, named *EPC* to the reader. If the reader correctly decodes the *EPC* sent by the tag, then this tag is successfully identified. Each tag performs the same identification procedure independently until all tags are successfully identified. Thus, it can be seen that if the reader fails in correctly decoding the tag reply signal (*RN16*, or *EPC*), then the tag will have to wait another reader command and then retransmit its reply signal.

Obviously, increasing of retransmissions will lead to degrading of the identification speed. Figure 8 shows the average number of EPC frame retransmissions when identifying 50 tags in repeated tests of 100 times. An average SNR $\overline{\gamma}$ range of 8 dB to 15 dB is selected since the minimum $\overline{\gamma}$ required for reliable decoding is 9 dB for Miller-coded RFID systems [22]. As shown in Figure 8, in distortion free and high SNR conditions, the average number of EPC frame retransmissions of the ZCD, CORR, and the MF demodulator are similar. However, when the channel is disturbed with severe amplitude distortions, the ZCD and the CORR demodulator show considerable increase of EPC frame retransmissions, while the MF demodulator demonstrates only a slight increasing number of retransmissions.

Figure 9 shows the evaluation results of the average tag-identification speed (tag/10 seconds). It can be seen from Figure 9 that the ZCD, CORR, and the MF demodulator show little performance difference in distortion-free and high SNR conditions. However, when the channel suffers severe amplitude distortions, the average tag-identification speed of the ZCD and the CORR demodulator degrade rapidly while the MF demodulator demonstrates a slight identification-speed degrading compared with the ZCD and the CORR demodulators.

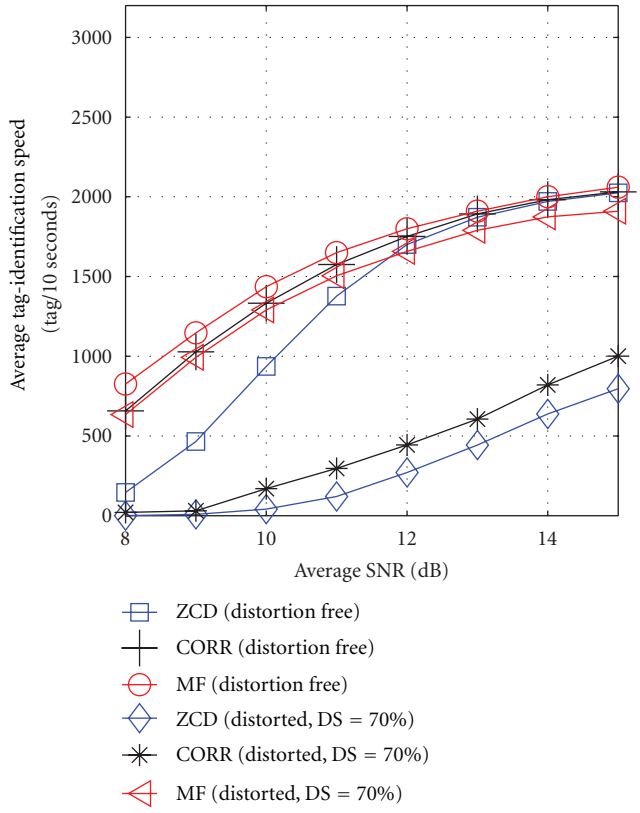

Figure 9: Average tag-identification speed (tag/10 seconds).

7. Implementation and Experiment Results

The designed Baseband MF demodulator was implemented on a Xilinx Virtex-4 LX100 FPGA in the UHF RFID reader platform developed by Samsung Techwin Co., Ltd. and RFID Research Center in Hanyang University. Figure 11 shows the

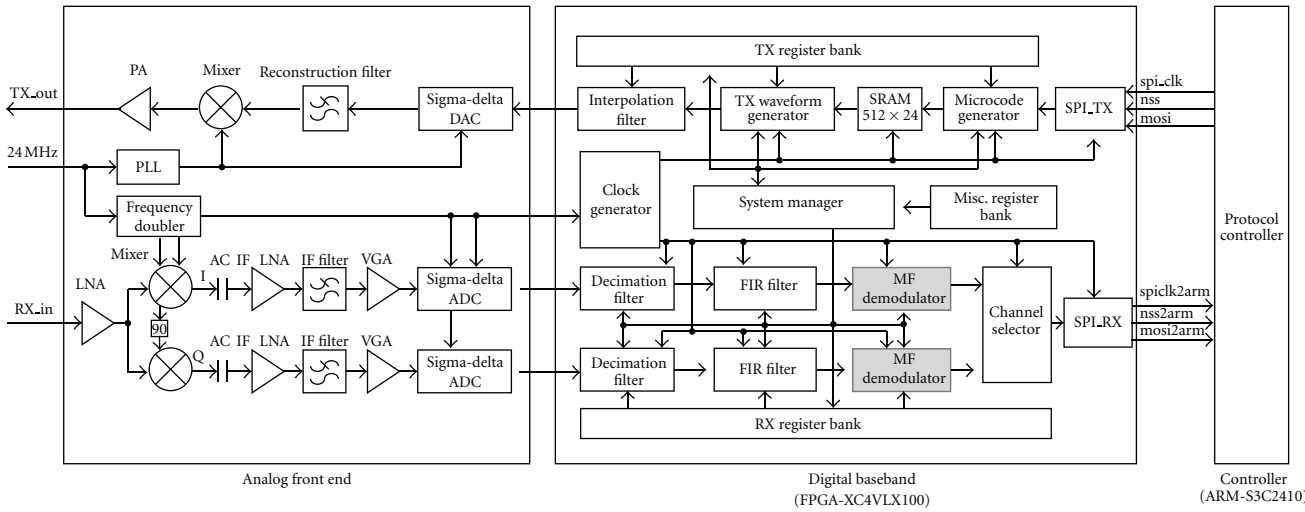

Figure 10: Top-level block diagram of the developed UHF RFID reader platform.

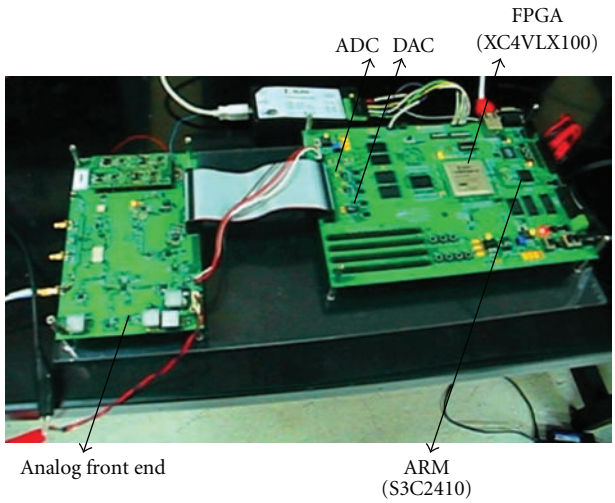

Figure 11: Implementation and verification platform (UHF RFID reader platform designed and prototyped by Samsung Techwin Co., Ltd. and RFID Research Center in Hanyang University, 2010).

photograph of the developed reader platform and Figure 10 depicts the internal architecture of the reader platform.

As can be seen from Figure 10, the platform consists of three main parts: the analog front end, the digital baseband (FPGA-XC4VLX100), and the controller (ARM-S3C2410). The analog front end up-converts baseband signal from the digital baseband and down-converts RF signal received from the antenna. The digital baseband is responsible for baseband modulation of the reader command signal and demodulation of the received tag-reply signal. The controller is the control unit that implements the Gen2 RFID protocol, and communicates with a host computer through Ethernet.

As shown in Figure 10, the transmitter (TX) up-mixer and DAC run on the 24 MHz clock while the receiver (RX) down-mixers, ADCs, and the digital Baseband work on a 48 MHz clock generated by a frequency doubler. In the digital baseband of the TX path, the baseband encoding and pulse shaping is achieved through a programmable lookup table. Thus, Baseband-modulated TX digital waveforms can be produced by interpreting commands received from the external protocol controller (ARM-S3C2410). In the digital baseband of the RX path, the I and Q signals sampled by the 48 MSPS ADCs are decimated by the data-rate-dependent decimation filters to reduce the sample rate. Following the decimation filter is the digital FIR filter which performs a band-pass filtering to provide additional DC suppression and out-of-band noise attenuation. After signal pre-processing, demodulation is performed by the proposed MF demodulator.

A top-level functional block diagram of the MF demodulator is shown in Figure 12. The power detector uses a noncoherent square-law detector which sums a number of squared samples and then compares with a threshold to determine whether a tag signal is present or not. Given detection of a tag-reply signal, the MF is enabled to provide SNR optimization of the tag reply signal. The implementation structure of the MF is shown in Figure 13. The MF is configured as an FIR filter with programmable coefficients. The filter length N is equal to the average number of samples over a half subcarrier period. The filter coefficients are set to unity to minimize hardware consumption.

Following the MF, a correlator-based preamble detector is then employed to search the preamble to arrive at the timing of the initial subcarrier symbol. After the preamble is found, an ML detector is used to perform symbol detection for tag subcarrier signals. The ML detector consists of a correlator bank and a symbol-decision block, and the structure is shown in Figure 14. As shown in Figure 14(a), the samples with a length of L in the filtered tag-reply signal $y_{\mathrm{MF}}(k)$ are correlated with reference waveforms $s(k)$ covering all possible frequency deviation within one subcarrier period. A comparator (as shown in Figure 14(b)) is then used to compare the correlation results and find

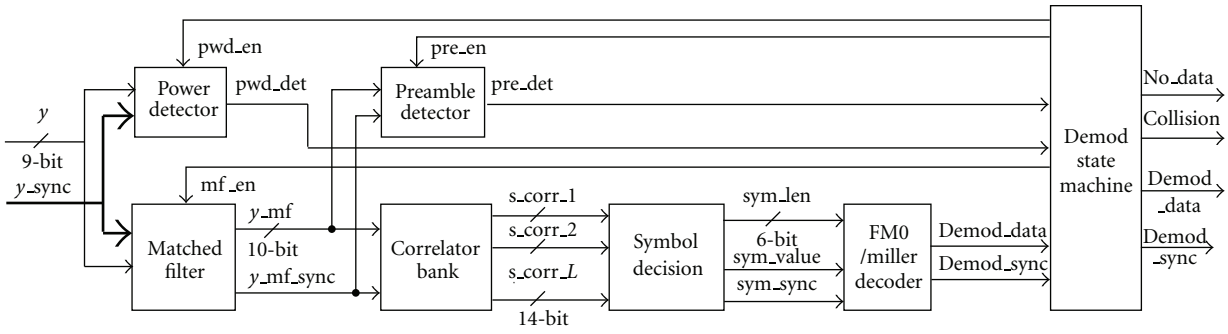

Figure 12: Block diagram of the MF demodulator.

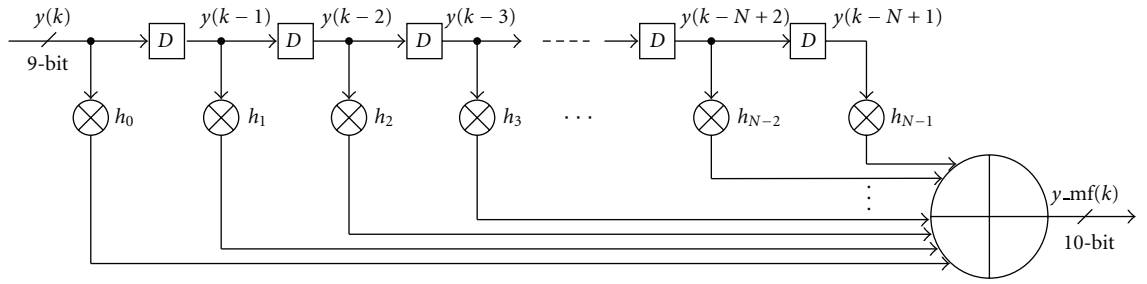

Figure 13: Structure of the MF.

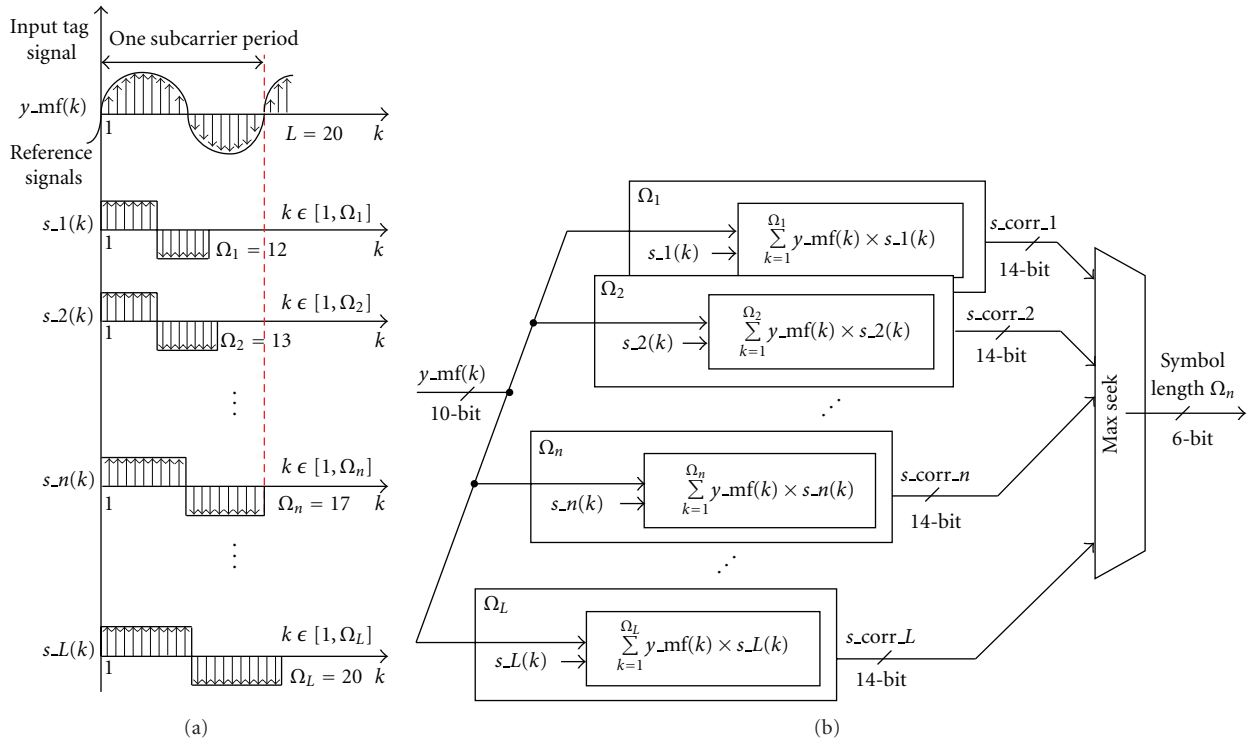

Figure 14: (a) Illustration of the reference signals in the correlator bank; (b) operation of the correlator bank and symbol-decision blocks.

the maximum value. Thus, the symbol type and length Ω is estimated as the same as that of the reference waveform producing the maximum correlation result. After the tag subcarrier symbols are detected, the FM0/Miller decoder block (as shown in Figure 12) is used to extract data from the symbols according to FM0-or Miller-encoding characteristics.

The proposed Baseband MF demodulator was implemented by VHDL code, which can be downloaded to the FPGA. Figure 15 shows the measurement results captured

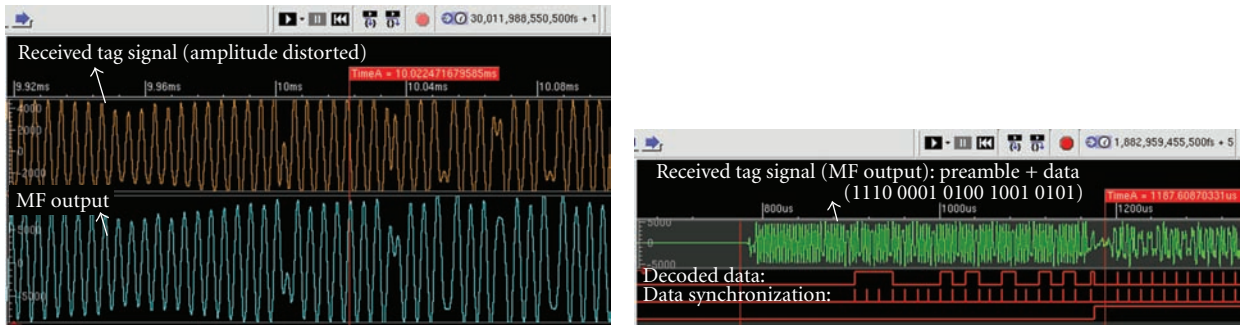

(a) (b)

Figure 15: FPGA implementation results of the baseband MF demodulator: (a) MF result; (b) symbol detector result.

by a logic analyzer. Figure 15(a) shows the implementation result of the MF. In Figure 15(a), the received tag reply signal is the practical tag reply signal (BLF = 300 kHz) received by the reader platform. The MF output is the filtering result of the received signal.

As can be seen from Figure 15(a), the amplitude distortions in the received signal are effectively compensated by the MF. Figure 15(b) shows the implementation result of the symbol detector. The input signal of the symbol detector is the MF output—the tag reply signal whose amplitude distortions have already been compensated by the MF. The decoded data in Figure 15(b) is the final output of the symbol detector. It can be seen that the data synchronization positions are exact, and the decoding result is correct.

We evaluated the practical performance of the implemented MF demodulator under AWGN conditions and the experimental setup is shown in Figure 16. In the experiment, the RFID reader platform is connected to a reader antenna with a height of 1.5 m to identify 64 RFID tags fixed at a distance of 1.5 m. The IDs and number of successfully identified tags are displayed on the host computer. An Agilent signal generator is used to generate AWGN noise, which propagates into the air through an isotropic antenna nearby the reader antenna.

For performance comparison, the ZCD was also implemented on the FPGA. By testing under different AWGN noise levels, we observed the following:

(1) At SNR = 9 dB, the average tag-identification speed of the ZCD was 24 tag/sec, while that of the MF demodulator was 66 tag/sec.

(2) At SNR = 8 dB, the average tag-identification speed of the ZCD was 7 tag/sec, while that of the MF demodulator was 30 tag/sec.

The experiment results verified the robustness of the proposed MF demodulator against signal distortion and noise disturbances. The difference of performance evaluation results between simulation and experiment is caused by the tag readability degradation in the practical environment. Tag readability mainly refers to the tag read range and read speed. Extensive investigations and measurements on the tag readability degradation factors in practical environments have been done in [24–26]. The tag readability relates to a

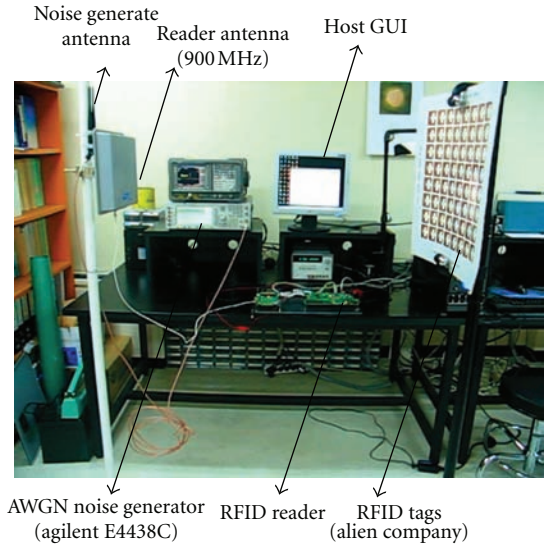

Figure 16: Experimental environment.

numerous number of factors, which could be classified as tag performance, reader setup, and operating environment. In practical environments, passive RFID tags usually demonstrate considerable performance variations. For example, the tag performance can be significantly affected by the relative position between the reader antenna and tag antenna. The distance and matching degree between the reader and tag antennas determine how much of the reader-transmitted RF power can be received by the tags.

In our experiment environment, the reader antenna is a directional antenna with a horizontal polarization pattern, while the tag antennas are dipole antennas. Since the tags are attached to a paper board with equal intervals, there exist differences in terms of distance and direction relative to the reader antenna among all the tags. These differences cause that the RF power received by the tags is different. In addition, the AWGN noise-generation antenna is an isotropic antenna. Unlike a directional antenna which propagates RF waves mainly in one direction, the isotropic antenna propagates RF waves in all directions. The polarization pattern of the noise-generation antenna determines that

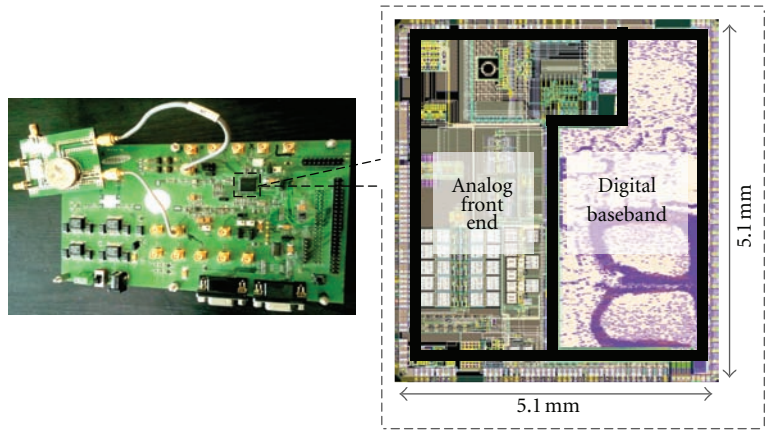

(a) (b)

Figure 17: (a) The complete UHF RFID reader platform with the reader chip embedded; (b) micrograph of the reader chip.

Table 2: Summary of the fabricated UHF RFID reader-chip characteristics and comparison with related works.

References	Technology	Protocol	Frequency	Tx power	Rx sensitivity	Power consumption	Area
[10]	0.18 μm SiGe BiCMOS	Gen2	860–960 MHz	+27 dBm	−85 dBm	1.2 W	21 mm^2
[18]	0.18 μm CMOS	Gen2	860–960 MHz	+10 dBm	−85 dBm	540 mW	36 mm^2
[23]	0.18 μm CMOS	Gen2	900 MHz	+4 dBm	−70 dBm	160.2 mW	23.85 mm^2
This work	0.18 μm CMOS	Gen2	860–960 MHz	+27 dBm	−90 dBm	1.08 W	26 mm^2

there could be differences in terms of received AWGN noise power between tags at different positions. Since tags at different positions receive different RF power from the reader antenna and different AWGN noise power from the noise-generation antenna, there could be some degree of readability differences among the tags. On the other hand in the simulation, since all the tags are given equal amount of signal power and AWGN noise power, the performance evaluation results of the simulation could be somewhat different from the experiment.

Finally, the complete RFID reader system containing the proposed Baseband MF demodulator was fabricated on a chip. The chip has a die size of 26 mm^2 and is fabricated using 0.18 μm CMOS technology.

Figures 17(a) and 17(b) show the constructed RFID reader platform using the chip and the chip micrograph, respectively. Table 2 shows the characteristics of the fabricated chip and comparison with other related works.

8. Conclusion

In this paper, a Baseband demodulator to compensate for signal distortions and estimate frequency deviations in passive UHF RFID systems is presented. The proposed Baseband demodulator is robust against strong signal distortions and noise, and also tolerates considerable frequency deviations. The validity and usefulness is verified by both computer simulation and implementation experiment. Based on the performance evaluation results, the proposed demodulator provides better reliability compared with the conventional demodulators. Moreover, since the high reliability of the proposed Baseband demodulator adds to some more logic cost, optimizing the implementation complexity and investigating more efficient implementation methods is our future research subject.

Acknowledgments

This work was supported by Korea Evaluation Institute of Industrial Technology (KEIT), under the R&D support program of Ministry of Knowledge Economy, Korea.

References

[1] E. K. B. Lee, C. Powell, and H. M. Kwon, "A novel wireless communication device with synchronized zero-crossing demodulator," in *Proceedings of the Global Telecommunications Conference (GLOBECOM '95)*, U.S. Patent Filed, Singapore, November 1995.

[2] H. M. Kwon, E. K. B. Lee, W. Hou, and Y. Bai, "New baseband zero-crossing demodulator for wireless communications, part—II: performance under fading channel," in *Proceedings of the Military Communications Conference (MILCOM '95)*, pp. 548–552, November 1995.

[3] T. Scholand and P. Jung, "Novel receiver structure for bluetooth based on modified zero-crossing demodulation," in *Proceedings of the IEEE Global Telecommunications Conference (GLOBECOM '03)*, pp. 729–733, December 2003.

[4] N. Dehaese, S. Bourdel, H. Barthélemy, Y. Bachelet, and G. Bas, "FSK zero-crossing demodulator for 802.15.4 low-cost receivers," in *Proceedings of the 12th IEEE International Conference on Electronics, Circuits and Systems (ICECS '05)*, pp. 1–4, Gammarth, Tunisia, December 2005.

[5] T. Scholand, A. Waadt, and P. Jung, "Novel bluetooth receiver structure deploying improved zero-crossing detection," *IEEE Transactions on Vehicular Technology*, vol. 56, no. 2, pp. 661–669, 2007.

[6] L. Zhang, S. Wang, T. Deng, and Z. Qin, "A novel demodulation method based on zero-crossing detection for UWB signal reception," in *Proceedings of the 5th International Conference on Wireless Communications, Networking and Mobile Computing (WiCOM '09)*, pp. 1–4, Wuhan, China, September 2009.

[7] P. Lajevardi, A. P. Chandrakasan, and H. Lee, "Zero-crossing detector based reconfigurable analog system," *IEEE Journal of Solid-State Circuits*, vol. 46, no. 11, pp. 2478–2487, 2011.

[8] S. J. Hwang, J. G. Lee, S. W. Kim et al., "A multi-protocol baseband modem processor for a mobile RFID reader," in *Proceedings of the International Conference on Embedded and Ubiquitous Computing*, pp. 785–794, Seoul, Korea, August 2006.

[9] D. H. Lee, K. Y. Jeon, and S. H. Cho, "Implementation of tag response data decoding algorithm for UHF RFID," in *Proceedings of the Korea Signal Processing Conference (KSPC '06)*, vol. 18, pp. 1–4, Cheonju, Korea, 2006.

[10] S. Chiu, I. Kipnis, M. Loyer et al., "A 900 MHz UHF RFID reader transceiver IC," *IEEE Journal of Solid-State Circuits*, vol. 42, no. 12, pp. 2822–2833, 2007.

[11] I. Mayordomo, R. Berenguer, A. Garcia-Alonso, I. Fernandez, and I. Gutierrez, "Design and implementation of a long-range rfid reader for passive transponders," *IEEE Transactions on Microwave Theory and Techniques*, vol. 57, no. 5, pp. 1283–1290, 2009.

[12] F. Ge and K. Choi, "Novel design and implementation for highly sensitive baseband protocol of Class-1 Generation-2 UHF RFID system," in *Proceedings of the IEEE International Conference on Electro/Information Technology (EIT '10)*, Chicago, Ill, USA, May 2010.

[13] P. Wei, B. Li, Y. Yang, H. Min, and J. Wang, "Synchronization with timing recovery loop in UHF RFID reader receivers," in *Proceedings of the IEEE International Conference on Electronics, Circuits, and Systems (ICECS '10)*, pp. 1148–1151, Athens, Greece, December 2010.

[14] Y. Liu, C. Huang, H. Min, G. Li, and Y. Han, "Digital correlation demodulator design for RFID reader receiver," in *Proceedings of the IEEE Wireless Communications and Networking Conference (WCNC '07)*, pp. 1666–1670, Kowloon , China, March 2007.

[15] C. Angerer and M. Rupp, "Advanced synchronisation and decoding in RFID reader receivers," in *Proceedings of the IEEE Radio and Wireless Symposium (RWS '09)*, pp. 59–62, San Diego, Calif, USA, January 2009.

[16] EPCglobal, "EPC radio-frequency identity protocols class-1 generation-2 UHF RFID protocol for communications at 860–960 MHz version 1.2.0," 2008.

[17] ETSI EN 302 208-1 V1. 1. 1, "European Telecommunications Standards Institute," 2004.

[18] P. B. Khannur, X. Chen, D. L. Yan et al., "A universal UHF RFID reader IC in 0.18-μm CMOS technology," *IEEE Journal of Solid-State Circuits*, vol. 43, no. 5, pp. 1146–1154, 2008.

[19] A. Ashry, K. Sharaf, and M. Ibrahim, "A compact low-power UHF RFID tag," *Microelectronics Journal*, vol. 40, no. 11, pp. 1504–1513, 2009.

[20] J.-H. Bae, J.-C. Kim, B.-W. Jeon et al., "Analysis of phase noise requirements on local oscillator for RFID system considering range correlation," in *Proceedings of the 4th European Radar Conference (EURAD '07)*, pp. 385–388, Munich, Germany, October 2007.

[21] H. Meyr, M. Moeneclaey, and S. A. Fechtel, *Digital Communication Receivers: Synchronization, Channel Estimation, and Signal Processing*, vol. 1, John Wiley & Sons, 1998.

[22] W. Wang, S. Lou, K. Chui et al., "A single-chip UHF RFID reader in 0.18 μm CMOS process," *IEEE Journal of Solid-State Circuits*, vol. 43, no. 8, pp. 1741–1754, 2008.

[23] I. Kwon, H. Bang, K. Choi et al., "A single-chip CMOS transceiver for UHF mobile RFID reader," in *Proceedings of the 54th IEEE International Solid-State Circuits Conference (ISSCC '07)*, pp. 216–598, San Francisco, Calif, USA, February 2007.

[24] J. Mitsugi and H. Hada, "Experimental study on UHF passive RFID readability degradation," in *Proceedings of the International Symposium on Applications and the Internet Workshops (SAINT '06)*, pp. 52–55, January 2006.

[25] P. V. Nikitin and K. V. S. Rao, "Performance limitations of passive UHF RFID systems," in *Proceedings of the IEEE Antennas and Propagation Society International Symposium (APS '06)*, pp. 1011–1014, Singapore, July 2006.

[26] A. Lázaro, D. Girbau, and D. Salinas, "Radio link budgets for UHF RFID on multipath environments," *IEEE Transactions on Antennas and Propagation*, vol. 57, no. 4, pp. 1241–1251, 2009.